An Experimental Investigation of Deformation and Fracture of Nacre–Mother of Pearl

F. Barthelat · H.D. Espinosa

Abstract Nacre, also known as mother-of-pearl, is a hard biological composite found in the inside layer of many shells such as oyster or abalone. It is composed of microscopic ceramic tablets arranged in layers and tightly stacked to form a three-dimensional brick wall structure, where the mortar is a thin layer of biopolymers (20–30 nm). Although mostly made of a brittle ceramic, the structure of nacre is so well designed that its toughness is several order of magnitudes larger that the ceramic it is made of. How the microstructure of nacre controls its mechanical performance has been the focus of numerous studies over the past two decades, because such understanding may inspire novel composite designs though biomimetics. This paper presents in detail uniaxial tension experiment performed on miniature nacre specimens. Large inelastic deformations were observed in hydrated condition, which were explained by sliding of the tablets on one another and progressive locking generated by their microscopic waviness. Fracture experiments were also performed, and for the first time the full crack resistance curve was established for nacre. A rising resistance curve is an indication of the robustness and damage tolerance of that material. These measurements are then discussed and correlated with toughening extrinsic mechanisms operating at the microscale. Moreover, specific features of the microstructure and their relevance to associated toughening mechanisms were identified. These features and mechanisms, critical to the robustness of the shell, were finely tuned over millions of years of evolution. Hence, they are expected to serve as a basis to establish guidelines for the design of novel man-made composites.

Keywords Biological material · Biocomposite · Tensile strength · Fracture · Toughening mechanisms

Introduction

Many biological organisms utilize hard tissues for structural support (i.e. human skeleton) or armor against external mechanical aggressions (i.e., sea urchin, seashells). Stiffness, which is a critical quality for these tissues, is achieved by incorporating mineral crystals into soft organic matrices [1]. However, incorporating hard and brittle inclusions into soft, resilient matrices also means that the material becomes more brittle and that its toughness drops significantly. Many examples of soft organic matrices saturated with mineral are indeed relatively brittle (tooth enamel, eggshell, prismatic seashell). Some hard mineralized biomaterials, however, seem not to follow this trend. The case of nacre from seashell is a typical example. Nacre is the material that composes the inner layer of many species of gastropods and bivalves. Made of 95% of aragonite (a form of $CaCO_3$, close to calcite), nacre is stiff ($E=60$–80 GPa) while maintaining a relatively high toughness ($J_{IC}=1.5$ kJ/m^2, this is about 1,000 times the toughness of aragonite). Compared with man-made ceramics, nacre is also less sensitive to internal defects and flaws [2, 3], and is relatively strong in tension (the highest tensile strength amongst all the materials used by seashells [4]). For these reasons nacre has been the focus of intense research for the

F. Barthelat (SEM Member)
Department of Mechanical Engineering, McGill University,
Montreal, Quebec H3A 2K6, Canada

H.D. Espinosa (✉, SEM Member)
Department of Mechanical Engineering, Northwestern University,
Evanston, IL 60208-3111, USA
e-mail: espinosa@northwestern.edu

past twenty years in the materials science community. Elucidating the exact microstructural features and mechanisms responsible for this high toughness and strength is quite relevant, because it may open the way to new generations of composite designed through *biomimetics* [5].

The high strength and toughness of nacre was first demonstrated by Currey and Taylor [4, 6]. Mechanical tests on nacre also included tensile strength tests [6], three and four point bending tests [3, 7], shear [3, 8, 9], compression [8, 10], microindentation [11] and nanoindentation [10, 12–14]. The toughness of nacre was typically characterized using single value toughness measurements [5], and work of fracture [6, 7]. Nacre is composed of microscopic polygonal tablets of aragonite, bonded together by a small fraction (5%) of organic materials (proteins, chitin [15]). The tablets are arranged in columns with some overlap as shown on Fig. 1. Under hydrated conditions the material is capable of relatively large inelastic deformations in tension, generated by the microscopic sliding of the aragonite tablets on one another. This mechanism is largely controlled by the interface. Previous analyses focused on mechanisms at the nanoscales at the interface (biopolymer [16], nano-asperities [3, 10, 17], mineral bridges [18]) and within the tablets themselves [13, 19]. How the structure of nacre controls its mechanical properties (stiffness, strength, toughness) has been the focus of several models [7, 17, 20–23]. Nacre is a material with a hierarchical structure, where mechanisms at distinct length scales contribute to the overall mechanical response. For example nanoscale mechanisms at the interfaces contribute to maintaining the cohesion of the tablets over large tablet separation distances, up to 500 nm [3, 16]. Likewise, specific toughening mechanisms operate at larger scales. Recently, through a combined experimental-numerical study we showed that at the microscale the waviness of the tablets is a key feature in the performance of nacre. Such tablet waviness enables progressive locking as the tablets slide on one another [9]. Micro and nanoscale mechanisms operate
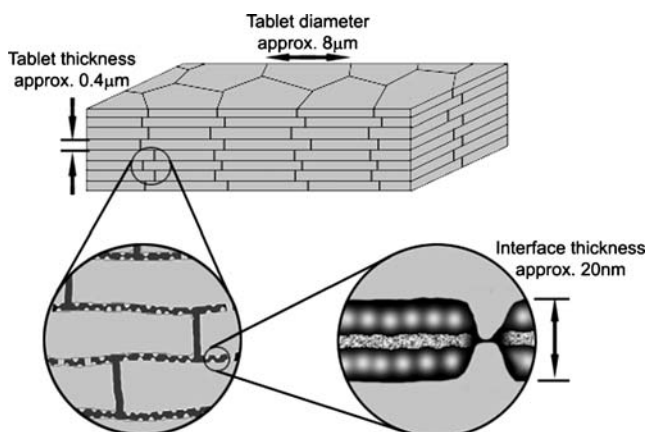
simultaneously and contribute to the mechanical performance observed at the macroscale. In the present paper, tensile experiments on dry and hydrated nacre are presented in detail. Nacre is capable of significant inelastic deformations and it is clear that linear fracture mechanics cannot capture nor represent the toughening processes of this material. The present paper presents fracture tests on nacre using techniques employed in materials with significant inelastic deformations to determine the full crack resistance curve. Likewise, nonlinear fracture mechanics models were used to correlate the rise in toughness with inelastic deformations around the crack tip and its wake. The relevance of the findings in the context of the microstructure of nacre and of potential bio-inspired materials is then discussed.

The Tensile Behavior of Nacre

Nacre in shells is always found as the inner layer of a two-layer armor system. The outer layer is made of hard, but more brittle calcite. There are several situations where the robustness of the shell relies on the tensile strength of nacre. For example a localized pressure, applied by a predator's bite or the impact of a rock displaced by currents or tidal waves, can be idealized as a point load normal to the shell. The outer layer is hard and prevents penetration, but as a result of the loading the overall shell experiences bending stress. In this case the outer layer is in compression, which is not a concern for the prismatic ceramic it is made of. On the other hand, the inside nacreous layer is in tension, which is often the loading mode leading to failure for ceramics. It is therefore critical for nacre to be strong in tension in the direction tangential to the shell, which is also the direction of the tablets. In the event of a more severe aggression the outside brittle layer may even completely fail, with cracks emanating from the point of impact (much like indentation on brittle materials, where cracks may emanate from the indenter's corners when a critical load is reached [2]). When the outside calcite layer is cracked, only the inner nacreous layer can maintain the integrity of the shell, which again involves nacre being strong in tension to resist forces that may pull the shell apart. For these reasons the strength and behavior of nacre in tension is critical to the robustness of the shell, and the behavior of nacre in tension has been central to numerous studies on nacre [3, 5–7, 24].

Specimen Preparation

In order to assess the behavior of nacre in tension, small dog bone shaped specimens were harvested from the nacreous layer of a red abalone shell. The specimen

Fig. 1 The structure of nacre
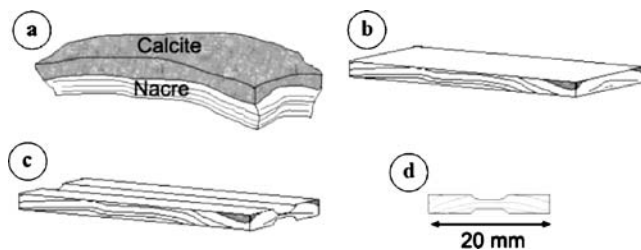
Fig. 2 Tensile specimen preparation: (**a**) Raw sample cut from the shell. (**b**) The calcitic layer was grinded away and the sample was lapped on both faces. (**c**) Grooves were machined on both sides (**d**) Slicing of the plate yielded the desired specimen geometry

preparation steps are depicted on Fig. 2. All the cutting and machining steps were performed in hydrated conditions. First, a 20 mm×50 mm strip was cut from the shell using a handsaw. The calcitic layer was removed on a grinding wheel, and the remaining nacre plate was grinded to make it roughly flat, with its faces aligned with the direction of the tablets. Both surfaces of the nacre plate were finished using a lapping machine with diamond slurry, in order to obtain flat and parallel faces. The next step was the machining of grooves on both sides of the plate, using a milling machine with a ball end mill. Finally, 1 mm thick slices were cut from the sample using a diamond saw to obtain the final specimen geometry. The overall length of the specimens was 20 mm, for a thickness of 0.6 mm. The gage section was 1.5 mm wide and 1.5 mm long. Such specimen contained about 3,000 tablets layers across the width, ensuring that the measured mechanical response does not depend on the size of the specimen. The deformations of the specimen subjected to tension were determined using digital image correlation [25, 26]. The method tracks dark and light features from one image to another (typically from a reference image to a deformed image), and requires some type of dark and light features on the specimen. In this case the surface of the sample was lightly scratched using a needle to produce a random pattern, as shown on Fig. 3. At the end of the preparation process, half of the specimens were stored in water to be tested in hydrated condition, while the other half was stored in ambient condition to be tested in dry condition.

Testing Procedure

The specimens were mounted on a miniature loading stage (Ernest F. Fullam, Inc, Latham, NY), which consists of two crossheads mounted on two threaded rods such that the crossheads move at the same rate, but in opposite directions [Fig. 4(a)]. A 400 N load cell (Honeywell Sensotec, Columbus, OH) was fitted on the frame for load measurements. The loading stage was placed under an optical microscope [Fig. 4(b)]. The specimens were loaded at a strain rate of about 0.001 s^{-1}, up to failure. The strain rate

was chosen to ensure "quasi-static" testing conditions. Higher strain rates were not explored at this point. During the test, the surface of specimen was maintained in focus, and pictures of the gage were taken at regular intervals. The strains in the specimen were determined using image correlation (VIC-2D, correlated solutions). After failure, pictures of the two broken pieces were acquired to determine strain recovery.

Tensile Experimental Results

Specimens were tested under both dry (ambient conditions) and hydrated conditions (soaked in water). Typical stress–strain curves are shown in Fig. 5(a) for four specimens. Dry nacre behaves like a monolithic ceramic and fails in a brittle fashion. The response is linear elastic ($E \sim 90$ GPa), up to a failure stress of 135 MPa (specimen #1) and 95 MPa (specimen #2). The behavior of dry nacre is similar to that of pure aragonite, also plotted on Fig. 5(a). By contrast, the behavior in hydrated condition exhibits a linear elastic response ($E \sim 80$ GPa), followed by a region of large strains starting at a stress of 70 MPa. The value of elastic modulus reported here in hydrated condition is slightly higher than the one previously measured on nacre from red abalone using three and four point bending [3], and higher than the modulus measured on nacre from *Pinctada* (oyster) using three-point bending [7]. These differences maybe explained by differences in experimental setup or specimen variations. As deformation progressed the material strain hardened, and the specimens failed at a strain of almost 0.01. Figure 6 shows the displacements and strain fields from the last image prior to failure. The deformations are distributed along the gage with no significant localization, and the
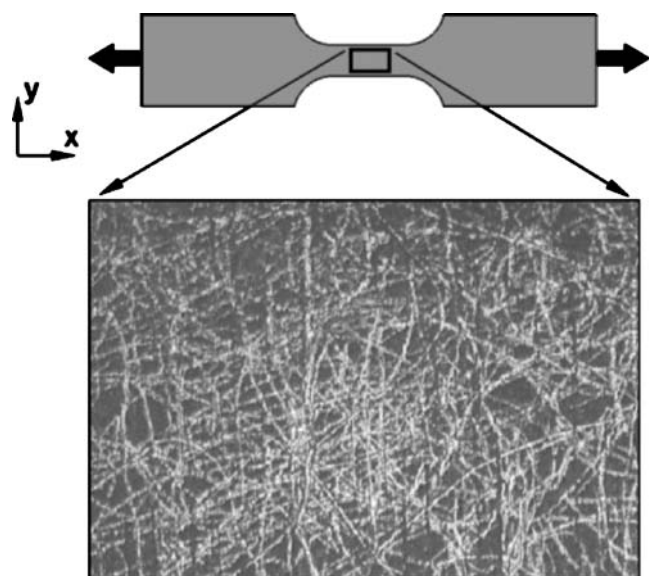
Fig. 3 Micrograph of a pattern of scratches on the surface of a nacre sample. The field of view is about 1.5 mm by 1 mm

Fig. 4 (a) Schematic of the miniature loading stage. (b) Picture of the experimental setting
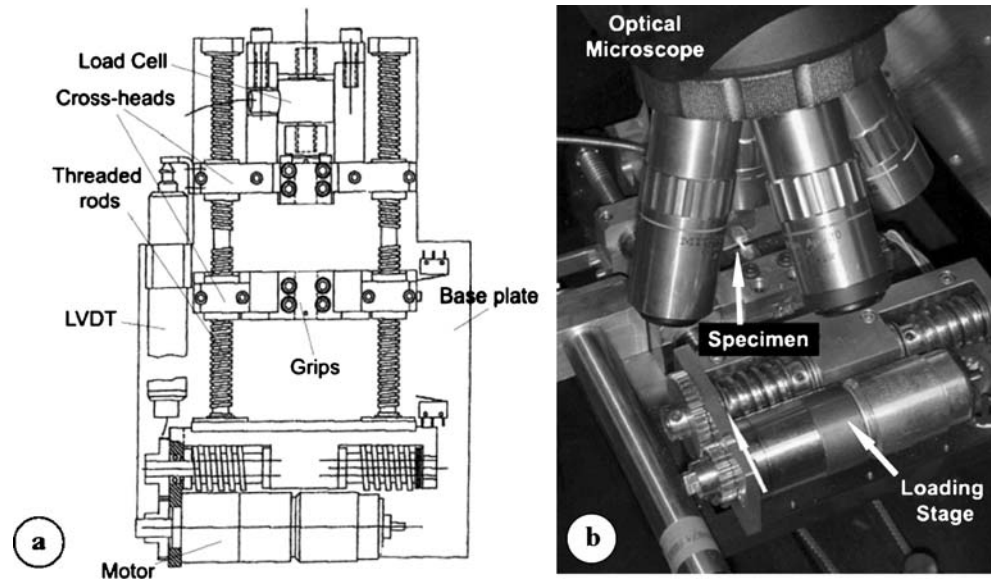

longitudinal strain reached local values of 0.015 prior to failure. Note that this is a significant level of deformation for a material mostly made of ceramic (monolithic ceramic typically fail at tensile strains of about 0.001). Note that in compression along the tablets nacre is stronger (at least 350 MPa), but also more brittle [3]. Compression across the tablets yields a lower modulus (about 30 GPa [10]) and a strength of about 500 MPa [10]. The weakest direction for nacre is tension across the tablets for which the strength is only about 15 MPa (Barthelat and Espinosa, 2006, unpublished research). Once unloaded, the material recovered about 50% of the total deformation. The unloading revealed that the modulus dropped to about 25 GPa, which is an indication of damage accumulations in the straining process. These relatively large deformations are generated through specific mechanisms. Tensile stresses are channeled from one column of tablets to the next, through shear stress in the overlap regions. When the shear strength of the interfaces is reached, the tablets start to slide on one another [Fig. 7(a)]. Upon tablet sliding, the observed decreased in modulus can probably be explained by a decrease in load transfer from tablet to tablet. A micrograph of a tested specimen shows that sliding exclusively occurs in the overlap regions and that at failure all the potential sliding sites were activated throughout the specimen gage [Fig. 7(b)]. Figure 7(c) shows separated tablets from a top view. Some ligaments of organic material, bridging the separated tablets, are still visible. Finally, Fig. 7(d) clearly shows that the fracture occurs along the interfaces, so that the prominent failure mode is tablet pullout. The transverse strains in the specimen were also determined. Figure 5(b) shows that initially the specimen contracts laterally, with Poisson ratios of $\nu=0.3$ under dry condition and $\nu=0.4$ in hydrated condition. Once tablet sliding was well established for the hydrated case (tensile strain>0.002), the transverse contraction ceased and a slight dilation was observed. From there, the transverse strains remained at the same value of about -0.001. No additional contraction due to Poisson's effects in the tablets was observed, probably because in this regime tablet sliding is the dominant mode of deformation and no additional strains are generated within the tablets. It is also possible that as the tablets slide on one another some dilation is generated in the transverse direction, which would counteract the Poisson's effect. Transverse expansion of the layers while they are sheared was also observed recently in simple shear tests on nacre [9].

Fig. 5 (a) Tensile stress strain curve for aragonite, nacre in dry condition and nacre in hydrated condition. (b) Corresponding transverse strain
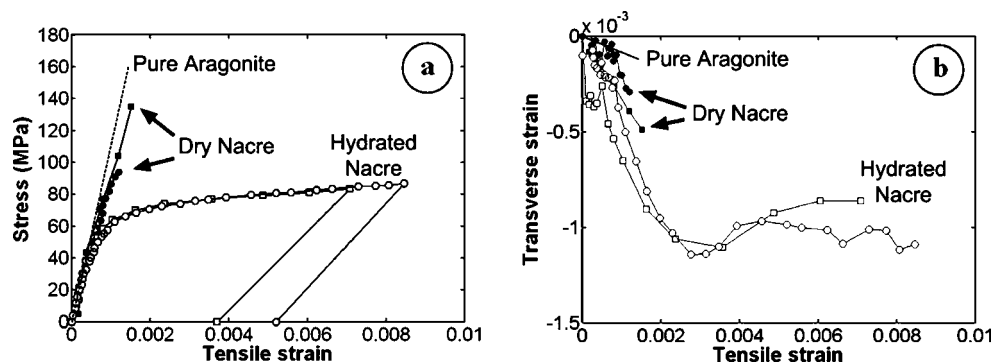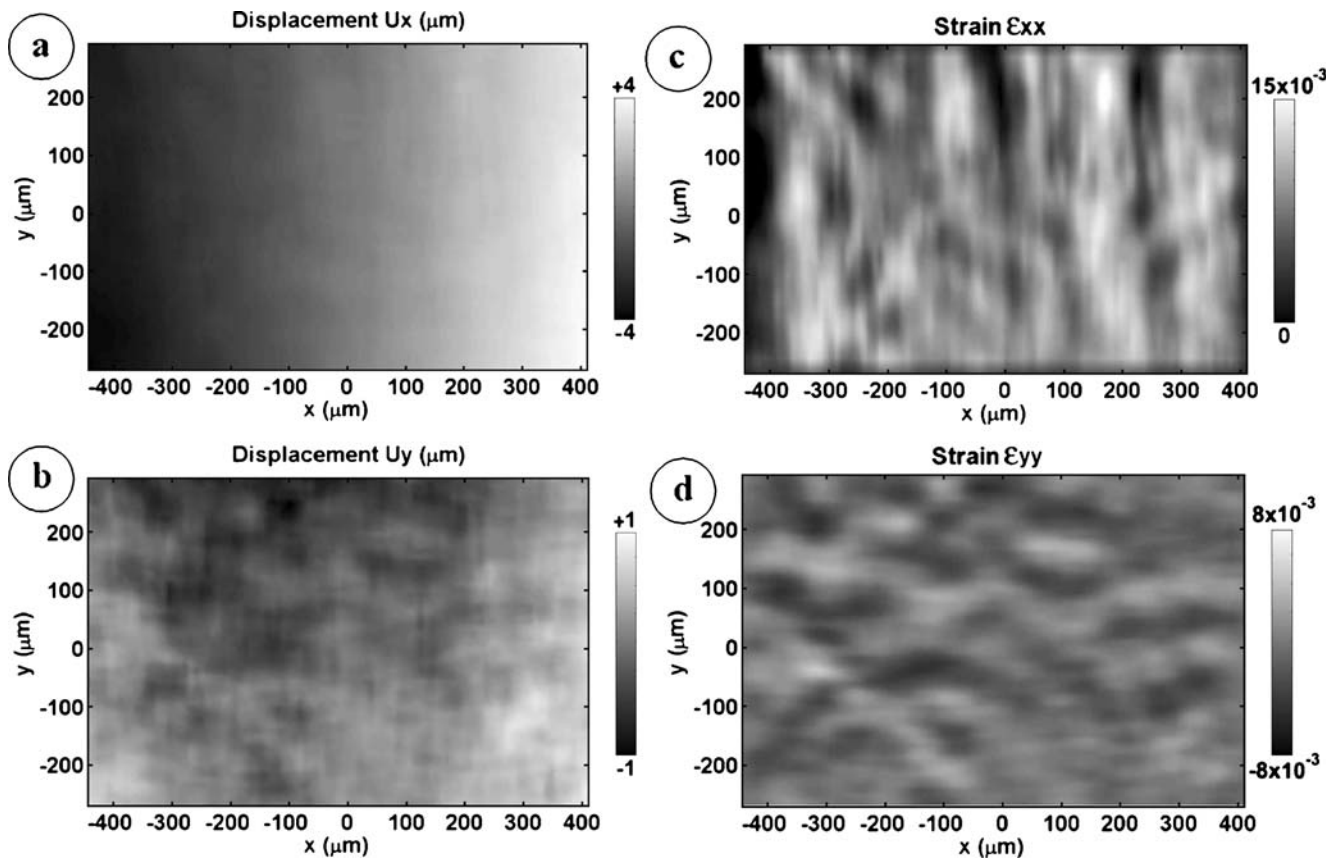
Fig. 6 Results from digital image correlation (reference image on image prior to failure were used). (**a**) and (**b**): Displacement fields in the gage. (**c**) and (**d**): ε_{xx} and ε_{yy} strain fields

The microstructure of nacre must be finely tuned in order to lead to such remarkable behavior in tension. For example, it is essential for the interfaces to be weaker than the tablets, so that tablet sliding is the primary deformation mechanism (as opposed to failure of the tablets, which would lead to a brittle behavior). Given a set of properties for the tablet and interface, this requirement can be met by tuning the overlap area with respect to the tablet thickness, while maximizing the mechanical energy absorbed by the material. Another requirement, more subtle but equally important, is that some hardening mechanism must take place at the local scale. When tablet sliding is initiated within the specimen in tension, sliding must require more and more stress (hardening) so that it is more favorable for the material to spread sliding and inelastic deformation, preventing localization and premature failure. This distribution of deformation was observed experimentally, and it is responsible for the large macroscopic deformations and hardening observed experimentally. In the mechanism of tablets sliding the tablets remain linear elastic, and therefore the hardening must be generated by mechanisms at the interfaces. Several features of the interfaces have the potential to generate local hardening. The biopolymer that binds the tablets is extremely resilient, and can sustain large deformation thanks to the molecular unfolding of modules

it contains [16]. This process, however, operates at more or less constant load, and could not account for the hardening observed experimentally [9]. Another potential source, the nanoasperities on the surface of the tablets may act as obstacles to tablet sliding. Such mechanism was proposed as the source of hardening in nacre [3, 27]. However, it was noted that while they may enhance the shear strength of the interface, nanoasperities are too small to generate hardening over the sliding distances observed experimentally [9, 10]. Recently, it was shown that the waviness of the tablets was the key feature that generates hardening in nacre [9]. Figure 8(a) is a scanning electron micrograph of polished nacre showing that in some locations, the waviness of the interface generates tablets that are thicker at their periphery. In two dimensions the shape is very similar to a dovetail, a locking device widely used in mechanical assembly. Many of these "dovetails" were observed in two-dimensional cross sections of nacre form red abalone. Strikingly, waviness and similar dovetail geometries can also be observed in nacre from other species of shells [14, 28–31]. When nacre undergoes tensile loading along the tablets, the dovetail geometry generates a tri-axial state of stress in the sliding region, with normal compression superimposed to shear [Fig. 8(b)]. The normal compression generates additional resistance to tablets sliding and
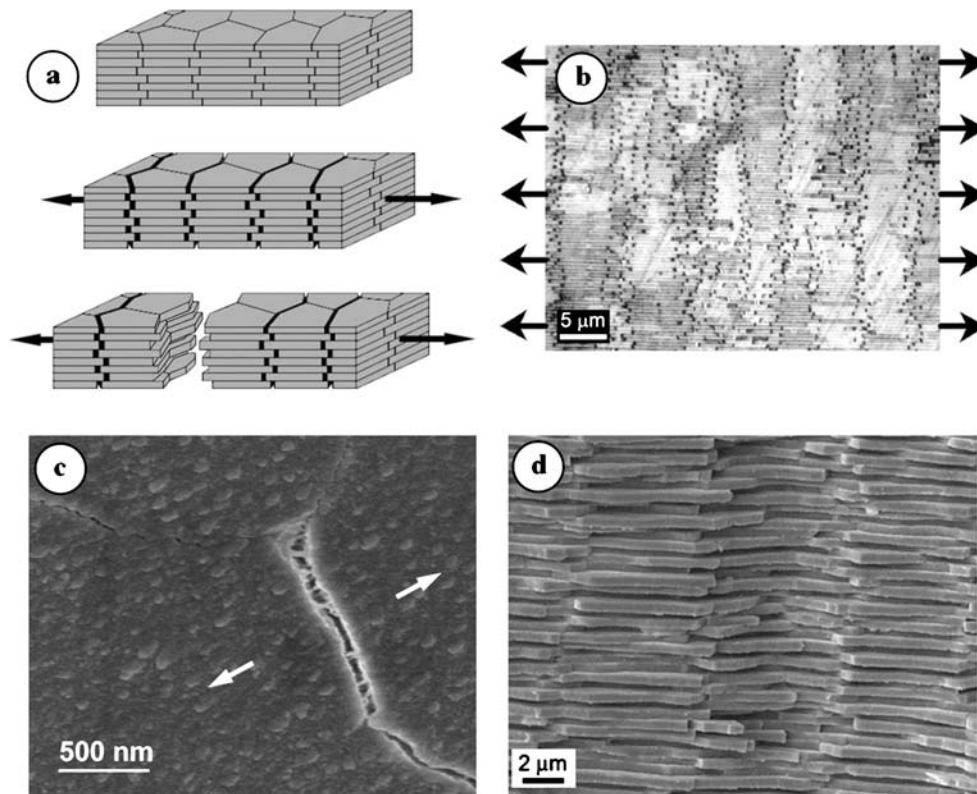
Fig. 7 (**a**) Schematic showing initial configuration, deformation and failure modes. (**b**) Micrograph of a post-mortem tensile specimen (Edge-on). The dark dots correspond to voids left by tablet separation. (**c**) SEM of a post-mortem tensile specimen (Face-on). Tablet separation can be seen, as well as ligaments. (**d**) Fracture surface of nacre showing that the failure occurs predominantly along the interfaces

pullout. It is noteworthy that equilibrium of forces at the interfaces requires tensile tractions at the core of the tablets. The biopolymer and mineral bridges are believed to play an important role in resisting these tensile forces, maintaining the integrity of the material. Dovetail geometries are often used in mechanical assemblies to interlock parts and generate extremely strong bonds between them. In nacre, however, the angle of the dovetails is very small (about 1–5°) so that the locking is weaker. Hence tablet pullout is possible, but accompanied by progressive locking and hardening. Recent numerical models actually demonstrated that even in the absence of hardening at the interface

material, the waviness of the tablets was able to explain the hardening rate observed experimentally [9]. After sliding distances of about 100–200 nm, the configuration becomes unstable and nacre fails by tablets pullout [as shown in Fig. 7(d)]. In closing we note that hardening and spreading of inelastic deformations has a significant impact on the toughness of nacre, as explained in the next section.

The Fracture of Nacre

The microstructure of nacre is not free of flaws. An examination under a microscope reveals large defect such
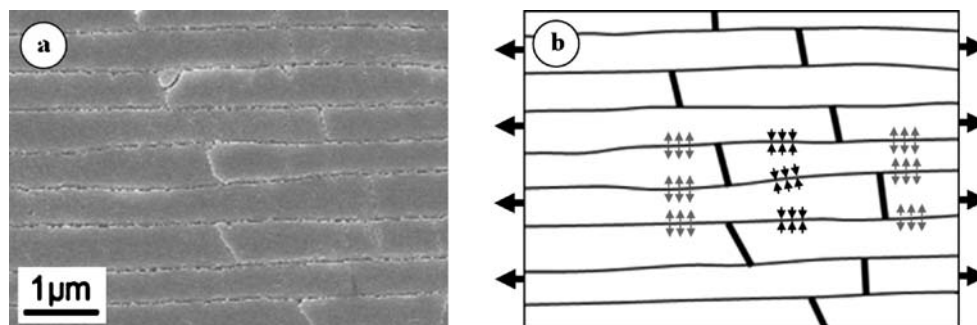
Fig. 8 (**a**) Scanning electron micrographs of a few dovetail like features at the periphery of the tablets. (**b**) Outline of the tablets contours, showing some of the stresses involved when nacre is stretched along the tablets. In addition to shear the interface is subjected to normal compression (*black arrows*), which generates resistance to tablet pullout. Equilibrium of forces at the interfaces requires tensile tractions at the core of the tablets

Fig. 9 Internal flaws in nacre: (**a**): Large pore (**b**) growth defects (stacking faults)
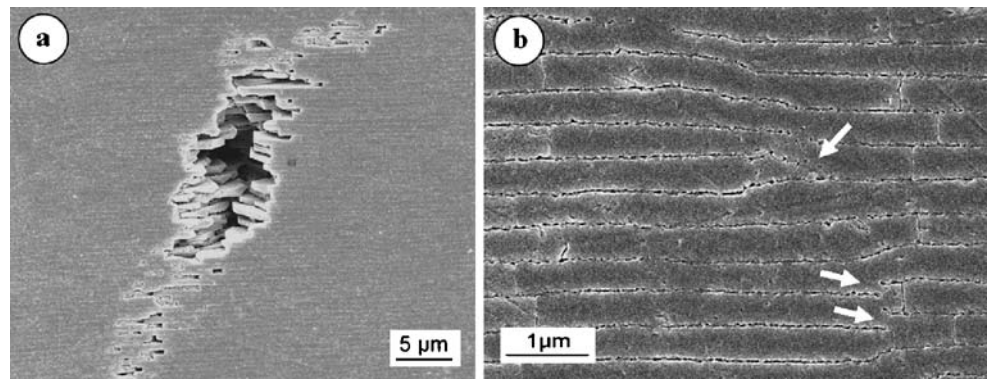
as pores, cracks and growth imperfections [Fig. 9]. When nacre is loaded in tension, these flaws become potential crack starters and resistance to cracking (toughness), is then a property that is essential for the robustness of the nacreous layer and of the shell as a whole. In this context, the relatively large inelastic deformations of nacre in tension are made possible by its toughness, in other words by its ability to resist cracking emanating from its initial flaws, making it damage tolerant [32].

The work of fracture of nacre was determined in the past for nacre from *Pinctada margaritifera* [6] along different directions, with the direction across the tablet being the toughest [6] (which is consistent with resisting cracks generated by tension along the tablets). So far, only single values of toughness were reported for nacre. While single toughness values properly characterize brittle materials with no toughening mechanisms, they might not be sufficient for nacre, because its impressive crack arrest capabilities [6] suggest more sophisticated, nonlinear failure mechanisms. In the present work stable crack growth and large inelastic regions were observed, and the full crack resistance curve was determined.

Preliminary Fracture Experiments

A preliminary fracture experiment was conducted using a nacre rectangular bar. A notch was machined with a diamond saw perpendicular to the plane of the tablets (a). The edge of the specimen was polished (down to 5 μm

Fig. 10 Polished notched sample under increasing load. (**a**) Initial frame (zero load) also showing the orientation of the tablets (**b**, **c**) Stationary crack, increasing inelastic zone. (**d**) crack advance, leaving a wake of inelastic deformations. The approximate crack tip position is marked with a black arrow
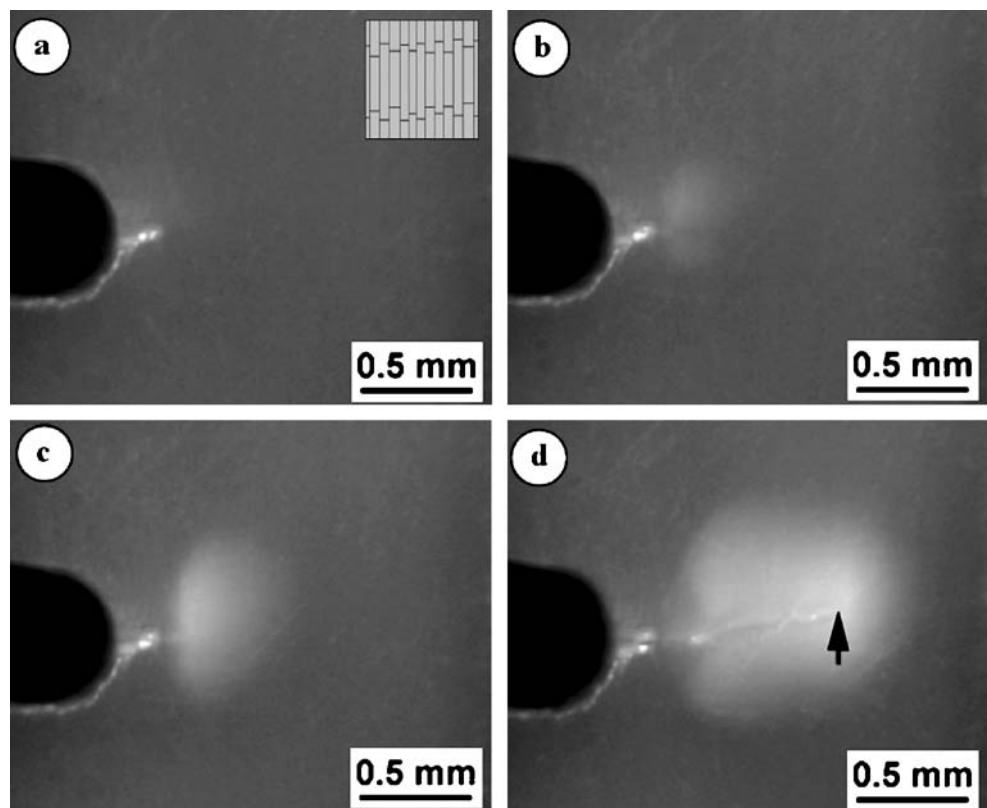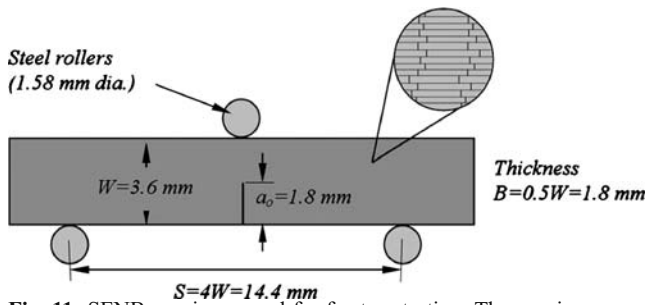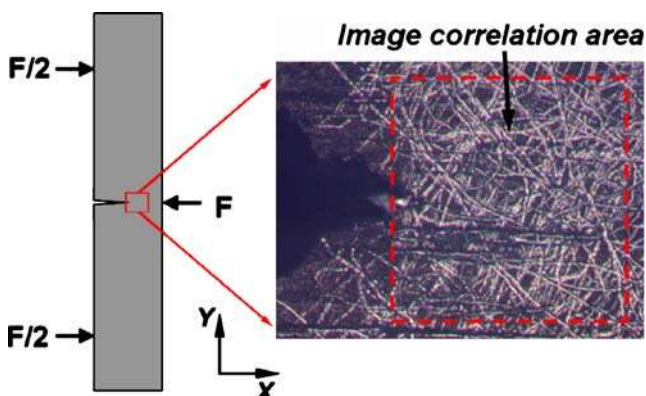
Fig. 11 SENB specimen used for fracture testing. The specimen was cut such that the notch is perpendicular to the tablets layers. Parts of the three point bending fixture are also shown

diamond slurry) and the notch was sharpened with a fresh razor blade. The specimen was loaded in bending in hydrated condition, using the miniature loading stage described in "The Tensile Behavior of Nacre" [Fig. 4(a)]. The specimen was imaged as the load was increased, and the resulting sequence of images is shown on Fig. 10.

As the load was increased, a white region formed ahead of the notch tip. Whitening for nacre has been identified as an indication of tablets sliding and inelastic deformation [3, 6]. The tablets, in the process of sliding apart, generate submicron size voids at their periphery that scatter white light and give a whiter appearance to the material (This optical phenomenon is similar to stress-whitening associated with crazing in polymers). As expected, tablet sliding and inelastic deformations initiate at the root of the notch, where tensile stresses are the highest. More strikingly, the inelastic region significantly increased in size before any crack growth was observed [Fig. 10(b, c) and Wang et al. [3]]. When the crack finally propagated, the inelastic zone had reached about 1 mm in width. The crack propagated in a very stable fashion, the process resembling stable tearing rather than brittle fracture. As the crack advanced it left a wake of inelastically deformed material on either sides of the crack faces [Fig. 10(d)]. Finally, after about 1 mm of crack extension the configuration became unstable and the specimen completely failed. The inelastic zone that appears

ahead of the crack tip and in the wake is commonly called process zone, and its associated mechanisms are central to some of the toughest of the engineering ceramics, such as zirconia [33, 34]. For the case of nacre the size of the process zone is remarkably large, which has two consequences. (1) Small scale yielding (s.s.y.) and linear elastic fracture mechanics (LEFM) approximations, as typically used in ceramics, are not valid for nacre (2) The high fracture toughness of nacre is probably associated with the formation of this process zone (which is detailed in the subsequent results section).
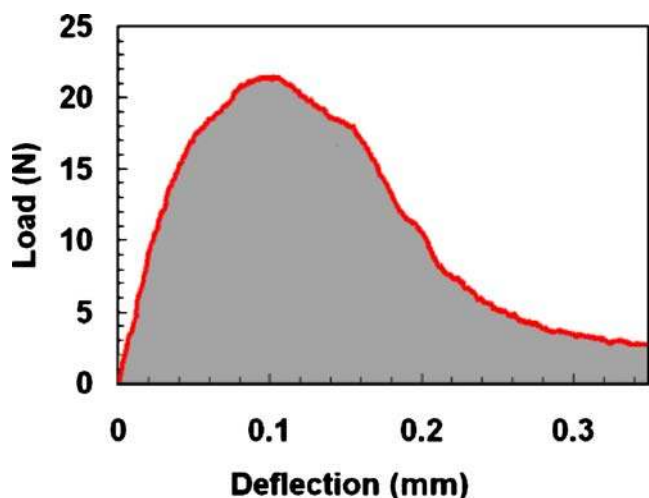
Fracture Specimens

The geometry and dimensions of fracture specimens must be chosen with care, so that the outcome of the experiment is indeed the fracture toughness of the material, a material property independent from specimen geometry. The condition for small scale yielding and K-dominance is for the fracture specimen to be at least 50 times larger than the inelastic region [35, 36]. In the case of nacre and based on the results reported in "Preliminary Fracture Experiments," such specimen would need to be at least 50 mm thick, which is not feasible from the 2–3 mm thick nacreous layer in the shell. Considering the large inelastic region associated with cracking nacre, nonlinear fracture mechanics and J must be used to model and characterize the material toughness. The condition for J-dominance for the single edge notch tensile specimen (SENT) is [35, 37]:

$$\text{All specimen dimensions} \quad \geq 200 \frac{J_Q}{\sigma_Y} \qquad (1)$$

For the Single edge notch bending (SENB) [35, 37]:

$$\text{All specimen dimensions} \quad \geq 25 \frac{J_Q}{\sigma_Y} \qquad (2)$$

Fig. 12 Specimen setup and micrograph of the specimen near the crack tip. Scratches provided features for image correlation

Fig. 13 Load deflection curve for a nacre SENB specimen

Fig. 14 Results from image
correlation: Displacements (**a**):
U and (**b**): *V*, and strains (**c**) ε_{yy},
(**d**) ε_{xx}, (**e**) ε_{xy}
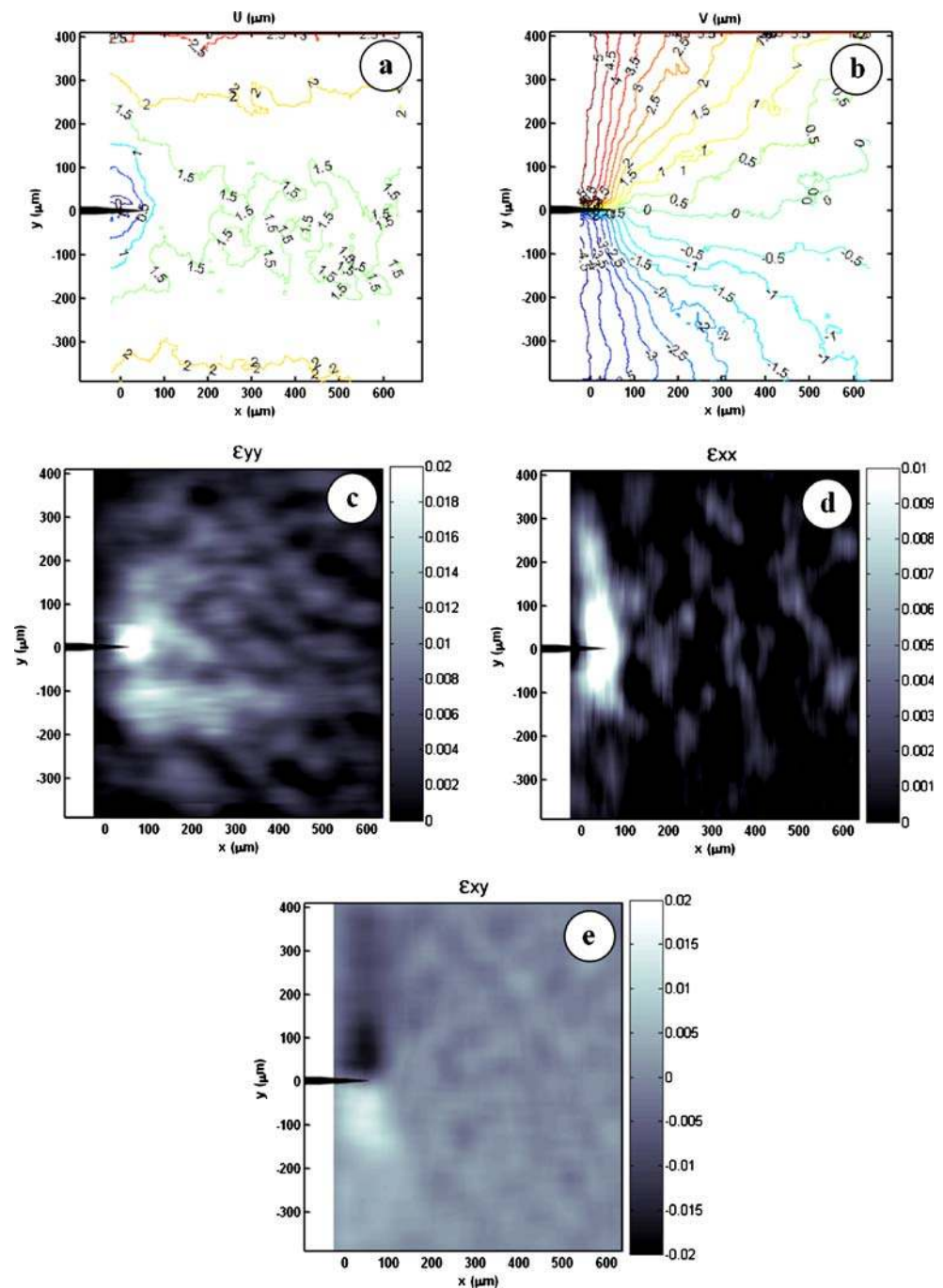
Given the constraints on specimen size for nacre, the SENB geometry was chosen. Testing standards for the fracture of ductile materials [38] also served as a guideline to determine the dimensions (width, depth, span, notch length) that will ensure a geometry-independent measure of the toughness. These dimensions are reported in Fig. 11. Note that the size of the specimen was as large as the thickness of the nacreous layer allowed. The specimens were cut so that the crack would propagate perpendicularly to the tablet layers. An initial rough notch was made by a diamond saw cut, and was then deepened using a razor blade until the

required depth was reached. Finally, a fresh razor blade was used to sharpen the notch. As for the tensile test, the surface of the specimen was lightly scratched to generate light and dark features required for digital image correlation [Fig. 12]. The specimens were stored in water and all fracture tests were performed in hydrated conditions.

Experimental Procedure

The three point bending fixture was mounted on the miniature loading stage described in "The Tensile Behavior

Fig. 15 (**a**): V displacement field, and line used for displacement collection. (**b**): Vertical displacements along the lines, with parabola fit for the determination of the crack tip location
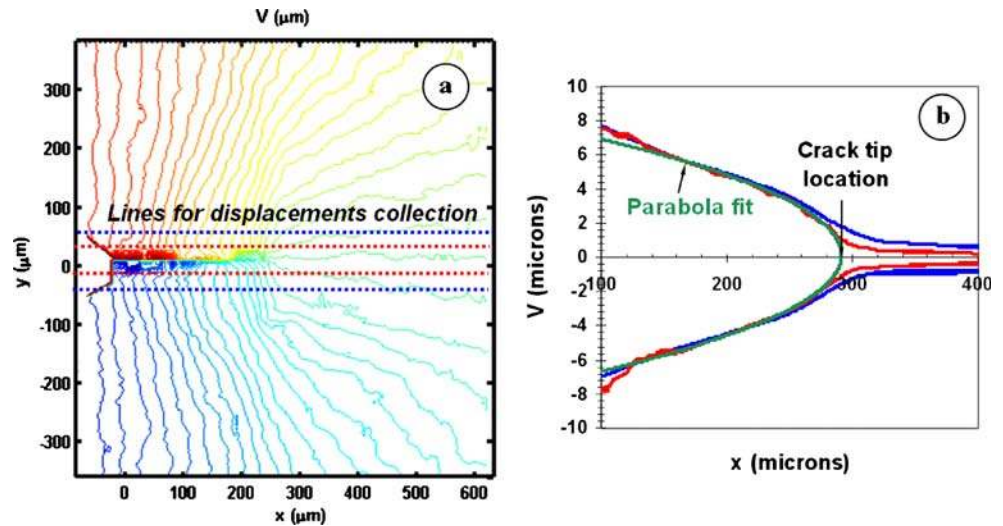
of Nacre." The crosshead displacement was measured with an LVDT, while the load was recorded using a 100 lbs load cell. The compliance of the loading stage was determined by inserting a thick block of steel in the fixture and by applying a compressive load. All the load-displacement curves from the actual test were corrected for machine compliance (C_m=0.4 μm/N). The stage was placed under an optical microscope during testing, and images of the surface of the specimen near the crack tip were recorded at regular intervals (Fig. 12). A typical load-deflection curve is shown in Fig. 13. Noteworthy is the bell shape of the load-deflection curve, a characteristic of stable crack propagation [35]. Figure 14 shows typical displacement and strain fields around the tip of an advancing crack obtained by digital image correlation. The tensile strain reached 0.02 near the crack tip, and upon crack advance a maximum strain of about 0.015 was measured in the wake, near the faces of the crack. While the crack tip cannot be directly detected visually, its position can be inferred from the displacement fields from image correlation.

Figure 14(a) and (b) show the displacement fields for an advancing crack. The vertical displacements were collected along several lines on either sides of the crack line, and parallel to it. Typical plots of the displacements along these lines are shown on Fig. 15(b). The displacement at the crack faces and normal to the crack path were assumed to follow parabolic profiles [Fig. 15(b)] and the intersection of the parabola with the crack line yielded the position of the crack tip. In some cases, it is possible to determine the applied stress intensity factor directly from the displacement fields [39, 40]. However in the present case this was not possible because nacre is non-linear and anisotropic, and no reliable constitutive law is available at this time (a constitutive law is needed to determine the stress field from

the displacements field). In order to determine the crack resistance curve, J was instead calculated from the applied load, specimen deflection, and instantaneous crack length. Note that the method borrows from existing standards [35, 38], but that it was adapted to take in account the elastic anisotropy of the material.

First, J is decomposed into an elastic contribution and a plastic contribution:

$$J = J_{\mathrm{el}} + J_{\mathrm{pl}}. \tag{3}$$

The elastic contribution J_{el} is based on linear elastic fracture mechanics:

$$J_{\mathrm{el}} = \frac{K_I^2}{E'}, \tag{4}$$

where K_I is the stress intensity factor (in mode I) and $E' = E/(1 - \nu^2)$ in plane strain for an isotropic material. For the orthotropic case [41]:

$$\frac{1}{E'} = \left(\frac{a_{11}a_{12}}{2}\right)^{1/2} \left(\left(\frac{a_{22}}{a_{11}}\right)^{1/2} + \frac{2a_{12} + a_{66}}{2a_{11}}\right)^{1/2} \tag{5}$$

with

$$a_{11} = \frac{1}{E_1}\left(1 - \frac{E_1}{E_2}\nu_{12}^2\right) \qquad a_{22} = \frac{1}{E_2}\left(1 - \nu_{23}^2\right)$$
$$a_{12} = \frac{1}{E_1}\frac{\nu_{12}}{1 + \nu_{23}} \qquad a_{66} = \frac{1}{G_{12}}. \tag{6}$$

Using the elastic constant for nacre (E_2=E_P=80 GPa; E_1= Ez=21 GPa; ν_{23}=νp=0.2; ν_{21}=νzp=0.2; G_{12}=Gzp=
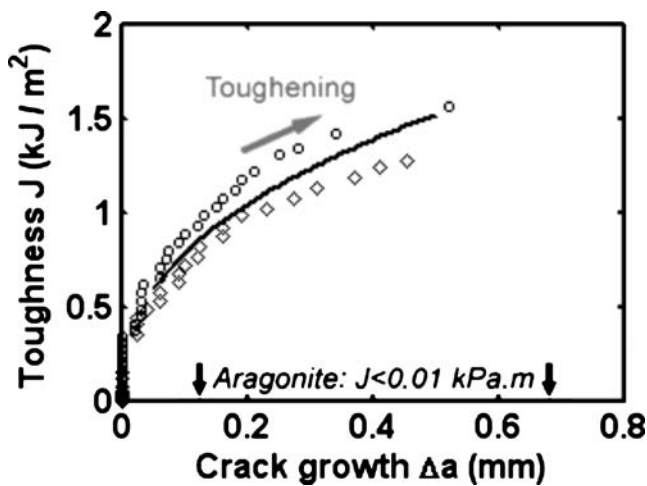
Fig. 16 Experimental crack resistance curves for nacre (from two experiments) with logarithmic function fit

10 GPa [10]), yields $E'=51$ GPa. For SENB specimens K_I is given by:

$$K_I = \frac{PS}{BW^{3/2}} f(a/W),\qquad(7)$$

where P is the applied load, S is the span, B is the specimen width and W is the specimen thickness. f is an non-dimensional function of the crack length a given by,

$$f(a/W) = \frac{3(a/W)^{1/2}\left[1.99 - (a/W)(1 - a/W)(2.15 - 3.93(a/W) + 2.7(a/W)^2)\right]}{2(1 + 2a/W)(1 - a/W)^{3/2}}\qquad(8)$$

For a non-growing crack in bend configuration J can be written as [35]:

$$J_{\mathrm{pl}} = \frac{2A_p}{Bb},\qquad(9)$$

where b is the ligament length $b = W - a$, and B is the specimen thickness. A_{p} is the plastic work, determined from the load-deflection curve and the unloading slopes. To take in account the fact that the crack is advancing and that the ligament b is continuously decreasing, an incremental definition of equation (9) was used [35]:

$$J_{pl(i)} = \left[J_{pl(i-1)} + \left(\frac{2}{b_{(i-1)}}\right)\left(\frac{A_{pl(i)} - A_{pl(i-1)}}{B}\right)\right]$$
$$\cdot \left[1 - \frac{a_{(i)} - a_{(i-1)}}{b_{(i-1)}}\right].\qquad(10)$$

Fracture Experimental Results

The resulting crack resistance curve, or J_R curve, is shown in Fig. 16 for two specimens. Crack growth starts at a J-integral value of $J_0=0.3$ kJ/m^2, which is already 30 times higher than the toughness of pure aragonite (about 0.01 kJ/m^2). As the crack advances, nacre becomes significantly tougher, with a significant tearing modulus (slope of the J_R curve). The maximum measured toughness was 1.5 kJ/m^2, which is five times the initial toughness. Note that upon crack advance, the material behind the tip unloads, which violates one of the conditions for the J-integral validity. However, it was demonstrated that under limited amounts of crack extension, J continues to characterize the state of stress at the crack tip as long as [35]:

$$\frac{W - a}{J}\frac{\partial J}{\partial a} = \omega \gg 1.\qquad(11)$$

This result was derived for metals but it is assumed to also be valid for nacre. Using the specimen dimensions and the experimental J_R curve, ones finds $\omega=5$ for $\Delta a\sim 0.15$ mm and $\omega=1$ for $\Delta a\sim 0.5$ mm. The crack resistance data for crack extensions larger than 0.5 mm was therefore discarded.

Single values for nacre toughness were reported in the past, ranging from 4 to 10 MPa.m$^{1/2}$ for red abalone [5]. Using equation (4) with $E'=58$ GPa, these values translate into a range of 0.3–1.7 kJ/m^2, which is consistent with the present results. The toughness measured here is also in the same range as the work of fracture measured in the past for nacre [6, 7]. For comparison, partially stabilized zirconia has a toughness of about $J_{IC}=0.4$ kJ/m^2 [2]. As discussed in previous work, testing conditions in laboratory and real life loading conditions can be quite different. It has been noted that the stiff testing machines in the laboratories do not store as much energy as predator jaws or crab pincers, which act as "soft machines" [1, 7]. In terms of fracture mechanics this means that an extending crack in nacre tends to be more stable in displacement-controlled conditions (stiff machine) than in load-controlled condition (soft, muscle actuated machine). However, this statement is true for any material. The crack resistance curve determined in this work for nacre is a material property, i.e., it does not depend on the specimen size, geometry or the loading conditions. It was also argued that although nacre had a high toughness, it was not suitable for crack arrest [1], as opposed to cross lamellar structures with lower toughness but better crack arrest capability [42]. It is true that very often a high toughness is not sufficient for reliability. A rising J_R curve means that existing flaws and cracks within the microstructure are stabilized. This is the case because the defects require more and more energy to propagate. The present work shows that nacre actually *does have* a pronounced rising crack resistance curve, which imparts damage tolerance and also explains the crack arrest performance observed by Currey [6]. In the following
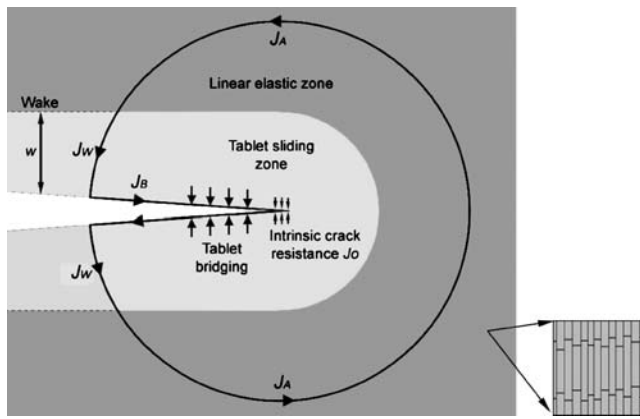
Fig. 17 Schematic showing a steady state crack in nacre, running across the tablets and leaving a wake of inelastically deformed material of width w. The J-integral contours are also shown

section, fracture mechanics models will be used to connect the measured J_R curve with the inelastic area around the crack, and with the microstructural features observed in nacre.

Extrinsic Toughening Mechanisms

The extrinsic contributions to toughening (mechanism that shield the crack tip remotely) will be examined in this section. Opening a crack in nacre involves tablet pullout across the crack faces, as suggested by the fracture surface [Fig. 7(d)]. The pullout forces generate crack face bridging, exerting forces that resist crack opening in a mechanism similar to that of fiber reinforced materials [2, 34]. In addition, a crack growing in nacre will generate new inelastic regions, which involves energy dissipation (so more energy is needed to propagate the crack). This toughening mechanisms, sometimes called process zone, is similar to transformation toughening [33] and to formation of microcracks clouds [27]. These two toughening contributions can be captured in a simple model using J-integral calculations along various parts of a contour [2]. The model assumes a crack in steady state, with a well

developed wake and bridging zone (the transient regime is more complicated and will not be discussed in this article). Figure 17 shows a two dimensional schematic of a crack in nacre, propagating across the layers. By combining the contributions of various sections of the contour it can be shown that [2]:

$$J_A = J_0 + J_B + J_W, \tag{12}$$

with J_A being the applied J, associated to loads applied to the system (i.e., loads applied on the specimen, remotely from the crack tip). J_o is the intrinsic toughness of nacre, in the absence of any other toughening mechanism. J_B is the contribution from crack bridging, i.e., from closure forces acting across the crack, and J_W is the contribution from the wake of the crack or process zone. From this equation, it is clear that only a part of the applied energy on the system is actually transmitted to the crack tip. In other words the extrinsic terms J_B and J_W are "shielding" the crack tip from remotely applied loads and effectively make the material tougher at the macroscale. The extrinsic terms were estimated by direct use of the J-integral definition, namely,

$$J = \int_\Gamma \left(W n_1 - T_i \frac{\partial u_i}{\partial x_1} \right) \mathrm{d}s. \tag{13}$$

The bridging term is given by,

$$J_B = \int_0^{2u} \sigma_{yy}(u)\, d(2u), \tag{14}$$

where the stress separation function $\sigma_{yy}(u)$ is the bridging stress acting across the interface as a result of tablet pullout distance u. The cohesive stress can be evaluated from the experimental tensile stress–strain curve. Assuming that the tablets are rigid and that their length is about $L_t = 7$ μm (from their average surface area):

$$2u \approx L_t \varepsilon_{yy}. \tag{15}$$

The pullout stress is simply the tensile stress from the tensile test. Figure 18(a) shows the tensile stress–strain curve from

Fig. 18 (**a**) Tensile stress strain curve. (**b**) Stress-separation function
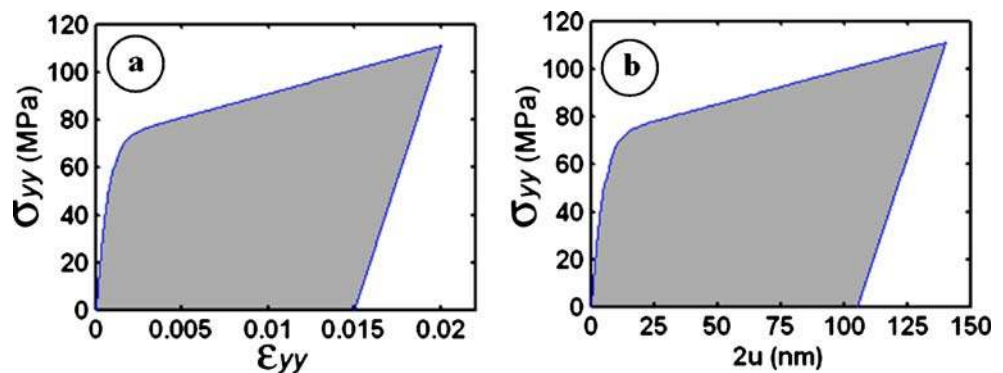
the experiment, which was extrapolated up to a strain of 0.02 to match the strains observed experimentally at the crack tip [see Fig. 14(c)]. Fig. 18(b) shows the stress-separation curve, obtained by transforming the strains using equation (15). The integral of equation (14) is then simply the area under the stress-separation curve, viz., $J_B=0.012$ kJ/m^2. This value is much smaller than the toughness measured experimentally. This suggests that while crack bridging by the tablets is evident from experimental observations, it actually has a minimal impact on the toughening of nacre.

The contribution from the process zone is now examined. It is written as:

$$J_W = 2 \int_0^w U(y)\mathrm{d}y, \tag{16}$$

where w is the half width of the wake, y is the distance from the crack plane and $U(y)$ is the energy density (i.e., the mechanical energy dissipated and stored per unit thickness) within the wake of the crack. By considering the energy dissipated by tension along the tablets, equation (16) becomes:

$$U(y) = \int_0^{\varepsilon_{yy}(y)} \sigma(\varepsilon)\mathrm{d}\varepsilon \tag{17}$$

Where $\sigma(\varepsilon)$ is the uniaxial response of nacre in tension along the direction of the tablets and $\varepsilon_{yy}(y)$ is the residual strain across the direction of the crack, away from the crack tip. Strain analysis in the wake of the crack revealed that the residual strain $\varepsilon_{yy}(y)$ in the wake increases linearly from zero at the boundary of the wake ($y=w$) to about 0.016 [43] at the edge of the crack. Using these values in equations (17) and (16), together with $w=0.5$ mm [Fig. 10(d)] one finds $J_W=0.75$ kJ/m^2, which is in the order of the rise in toughness observed experimentally. Other dissipative deformation modes, not capture in the simplified model, also contribute to the raise in toughness. This important result shows that the formation of inelastic regions in cracked nacre is the source of toughening: Advancing a crack in nacre involves the formation of a zone of large inelastic deformations from "virgin" material ahead of the tip. At the same time, the material behind the tip has been unloaded but an irreversible deformation remains. The energy consumed in this process is captured by the model [equation (16)]. Its origin is probably viscoplastic dissipation at the biopolymer in the interface. Note that the toughening is promoted by a large inelastic region and the spreading of tablet sliding, which is made possible by local hardening and tablet waviness (through progressive "dovetail" locking) as previously explain in "Tensile Experimental Results."

Lastly, note that in the fracture experiment the propagation of the crack did not seem to have reached the steady state; which may require several millimeters of crack growth to be attained. For the case of zirconia, models predict that the steady state regime is reached for crack growths equal to about five times the half width of the process zone [33]. For nacre, the same guideline predicts that a crack would reach steady state after a 2.5 mm extension, which seems to be consistent with the trend of Fig. 16. Once the steady state is reached, no additional toughening occurs. This leads to unstable configurations for the crack, and potentially catastrophic failure. The nacreous layer, however, is only about 1–3 mm thick for red abalone, and even thinner for other species. This means that a crack within the nacreous layer of the shell might actually never reach the steady state regime and will always tend to be stabilized.

Conclusions

Nacre is amongst the strongest of the materials found in seashells, and it has a remarkable toughness despite being mostly made of a brittle ceramic. In order to characterize its mechanical performance, tensile and fracture tests were performed on nacre from the shell red abalone (*Haliotis rufescens*). Millimeter size specimens, miniature loading stage and non-contact optical methods were used in the experiments. The tensile tests highlighted the relatively large inelastic tensile deformations in nacre (at the condition that it is hydrated). These deformations are generated by the microscopic mechanism of tablet sliding, and by the progressive "dovetail-type" locking made possible by their waviness. The same type of inelastic deformations was found in large regions ahead and behind advancing cracks in nacre. Instead, experimental approaches based on nonlinear fracture mechanics revealed a rising crack resistance curve, which is the characteristic of a material that can stabilize and even arrest cracks. The prominent fracture toughening mechanism in nacre was found to be viscoplastic energy dissipation at the biopolymer between tablets, associated with the sliding of the tablets on one another. Advancing a crack though nacre means that virgin material ahead of the tip must deform inelastically, which consumes a significant amount of energy. For this process to have an impact, the inelastic region must spread over large volumes around the crack, which is made possible by the local hardening and progressive locking generated by tablet waviness. While this result yields a new understanding on the source of toughness for nacre, the synergy of mechanisms operating at nano, micro and mesoscales has yet to be captured with combinations of small-scales experiments and multiscale

modeling. Such sophisticated microstructures and mechanisms have been finely tuned over millions of year of evolution, in animals that rely on the robustness of their shell for survival. These findings are likely to inspire new composite materials, through biomimetics.

References

1. Currey, JD (1999) The design of mineralised hard tissues for their mechanical functions. J Exp Biol 202:3285–3294.
2. Lawn BR (1993) Fracture of brittle solids. Cambridge University Press, New York.
3. Wang RZ, Suo Z, Evans AG, Yao N, Aksay IA (2001) Deformation mechanisms in nacre. J Mater Res 16:2485–2493.
4. Currey JD, Taylor JD (1974) The mechanical behavior of some molluscan hard tissues. J Zool (London) 173:395–406.
5. Sarikaya M, Aksay IA (eds) (1995) Biomimetics, design and processing of materials. Woodbury, NY.
6. Currey JD (1977) Mechanical properties of mother of pearl in tension. Proc R Soc Lond 196:443–463.
7. Jackson AP, Vincent JFV, Turner RM (1988) The mechanical design of nacre. Proc R Soc Lond 234:415–440.
8. Menig R, Meyers MH, Meyers MA, Vecchio KS (2000) Quasi-static and dynamic mechanical response of haliotis rufescens (abalone) shells. Acta Mater 48: 2383–2398.
9. Barthelat F, Tang H, Zavattieri PD, Li CM, Espinosa HD (2007) On the mechanics of mother-of-pearl: a key feature in the material hierarchical structure. J Mech Phys Solids 55:225–444.
10. Barthelat F, Li CM, Comi C, Espinosa HD (2006) Mechanical properties of nacre constituents and their impact on mechanical performance. J Mater Res 21:1977–1986.
11. Wang RZ, Wen HB, Cui FZ, Zhang HB, Li HD (1995) Observations of damage morphologies in nacre during deformation and fracture. J Mater Sci 30:2299–2304.
12. Barthelat F, Espinosa HD (2005). In: MRS 2004 fall meeting. Boston.
13. Li XD, Chang WC, Chao YJ, Wang RZ, Chang M (2004) Nanoscale structural and mechanical characterization of a natural nanocomposite material: the shell of red abalone. Nano Lett 4:613–617.
14. Bruet BJF, et al. (2005) Nanoscale morphology and indentation of individual nacre tablets from the gastropod mollusc Trochus niloticus. J Mater Res 20:2400–2419.
15. Schaeffer TE, et al. (1997) Does abalone nacre form by heteroepitaxial nucleation or by growth through mineral bridges? Chem Mater 9:1731–1740.
16. Smith BL, et al. (1999) Molecular mechanistic origin of the toughness of natural adhesives, fibres and composites. Nature (London) 399:761–763.
17. Evans AG, et al. (2001) Model for the robust mechanical behavior of nacre. J Mater Res 16:2475–2484.
18. Song F, Bai YL (2003) Effects of nanostructures on the fracture strength of the interfaces in nacre. J Mater Res 18:1741–1744.
19. Li XD, Xu ZH, Wang RZ (2006) In situ observation of nanograin rotation and deformation in nacre. Nano Lett 6:2301–2304.
20. Kotha SP, Li Y, Guzelsu N (2001) Micromechanical model of nacre tested in tension. J Mater Sci 36:2001–2007.
21. Katti K, Katti DR, Tang J, Pradhan S, Sarikaya M (2005) Modeling mechanical responses in a laminated biocomposite. Part II. Nonlinear responses and nuances of nanostructure. J Mater Sci 40:1749–1755.
22. Okumura K, de Gennes PG (2001) Why is nacre strong? Elastic theory and fracture mechanics for biocomposites with stratified structures. Eur Phys J, E Soft Matter 4:121–127.
23. Gao HJ (2006) Application of fracture mechanics concepts to hierarchical biomechanics of bone and bone-like materials. Int J Fract 138:101–137.
24. Katti DR, Katti KS (2001) Modeling microarchitecture and mechanical behavior of nacre using 3D finite element techniques. Part 1. Elastic properties. J Mater Sci 36:1411–1417.
25. Peters WH, Ranson WF (1982) Digital imaging techniques in experimental stress-analysis. Opt Eng 21:427–431.
26. Chu TC, Ranson WF, Sutton MA, Peters WH (1985) Applications of digital-image-correlation techniques to experimental mechanics. Exp Mech 25:232–244.
27. Evans AG, et al. (2001) A model for the robust mechanical behavior of nacre. J Mater Res 16:2475–2484.
28. Manne S, et al. (1994) Atomic-force microscopy of the nacreous layer in mollusk shells. Proc R Soc Lond, B Biol Sci 256:17–23.
29. Feng QL, Cui FZ, Pu G, Wang RZ, Li HD (2000) Crystal orientation, toughening mechanisms and a mimic of nacre. Mater Sci Eng, C Biomim Mater, Sens Syst 11:19–25.
30. Song F, Bai Y (2002) Nanostructure of nacre and its mechanical effects. Int J of Nonlinear Sci & Numer Simul 3(3):257–260.
31. Blank S, et al. (2003) The nacre protein perlucin nucleates growth of calcium carbonate crystals. J Microsc-Oxford 212:280–291.
32. McNulty JC, Zok FW, Genin GM, Evans AG (1999) Notch-sensitivity of fiber-reinforced ceramic-matrix composites: effects of inelastic straining and volume-dependent strength. J Am Ceram Soc 82:1217–1228.
33. McMeeking RM, Evans AG (1982) Mechanics of transformation-toughening in brittle materials. J Am Ceram Soc 65:242–246.
34. Evans AG (1990) Perspective on the development of high-toughness ceramics. J Am Ceram Soc 73:187–206.
35. Saxena A (1998) Nonlinear fracture mechanics. CRC Press, Boca Raton, FL.
36. ASTM (2005) Standard E399-05: standard test method for linear-elastic plane-strain fracture toughness KIc of metallic materials.
37. McMeeking RM, Parks DM (1979) In: Elastic-plastic fracture, vol 668, pp 175–194. American Society for Testing and Materials (ASTM-STP), Philadelphia.
38. ASTM (2004) ASTM standard E 1820-01: Standard test method for measurement of fracture toughness.
39. Barker DB, Sanford RJ, Chona R (1985) Determining K and related stress-field parameters from displacement-fields. Exp Mech 25:399–407.
40. McNeill SR, Peters WH, Sutton MA (1987) Estimation of stress intensity factor by digital image correlation. Eng Fract Mech 28:101–112.
41. Sih GC, Paris PC, Irwin GR (1965) On cracks in rectilinearly anisotropic bodies. Int J Fract Mech 1:189–203.
42. Kamat S, Su X, Ballarini R, Heuer A (2000) H. Structural basis for the fracture toughness of the shell of the conch Strombus gigas. Nature 405:1036–1040.
43. Barthelat F, Tang H, Li C, Espinosa H (2007) On the microscopic origins of the toughness of nacre (submitted).